

# Analysis of Shear Lag Effect of Steel-Concrete Composite Box Girders with Straight Steel Webs

Hua Luo, Jianqiang Feng, Qincong She, Bin Li, Changqing Wu and Yongqing Zeng, *Member, IAENG*

**Abstract**—The study presents an analysis of steel-concrete composite box girders with straight webs. A composite girder specimen is designed and tested. Analytical strain solutions for the composite girders under mid-span concentrated load are derived using the energy variation method, and the resulting strains on the top surface of the concrete slab are computed. A comparative analysis is conducted to verify the reliability of the analytical solutions. Furthermore, the investigation delves into the impact of several parameters on the strain distribution of the concrete top surface, including the ratio of elastic modulus, thickness of the concrete slab, calculation span of the composite girder, the ratio of the cantilever slab width to the half-width of the top slab ( $b_2/b_1$ ), thickness of the upper flange plate of the steel beam, and thickness of the web plate of steel beam. The study reveals that the ratio of the elastic modulus and thickness of the web plate has insignificant effects on the shear lag effect of the composite girder. Increasing thickness of the concrete slab proves to be effective in reducing the shear lag effect. Increasing thickness of the upper flange plate of the steel beam weakens the shear lag effect, whereas a longer calculation span has a more significant impact on the strain distribution of further sections from the loading point. Furthermore, the study indicates that when the  $b_2/b_1$  ratio is less than 1, it has a tiny impact on the shear lag effect; however, when the  $b_2/b_1$  ratio is greater than 1, the shear lag effect becomes more pronounced with increasing  $b_2/b_1$ . The results of the analysis can provide references for similar designs and constructions of composite structures.

**Index Terms**—steel-concrete composite girder, shear lag effect, energy variational principle, strain distribution, parameter impact analysis

Manuscript received July 14, 2023; revised January 8, 2024. This work was supported by the Natural Science Foundation of Hunan Province, China (Grant No. 2022JJ40160), the Program of Hunan Province Education Department (Grant Nos. 23A0496, 23B0645 and 22A0472), the Postgraduate Research Innovation Project of Hunan Institute of Science and Technology, China (Grant No. YCX2023A51), and the College Students' Innovation and Entrepreneurship Training Program of Hunan Institute of Science and Technology, China (Grant No. [2023]46-79).

Hua Luo is an associate professor in College of Civil Engineering and Architecture, Hunan Institute of Science and Technology, Yueyang, 414000, China, (e-mail: 12015024@hnist.edu.cn).

Jianqiang Feng is a postgraduate student in College of Civil Engineering and Architecture, Hunan Institute of Science and Technology, Yueyang, 414000, China, (e-mail: 822211140531@vip.hnist.edu.cn).

Qincong She is a lecturer in College of Civil Engineering and Architecture, Hunan Institute of Science and Technology, Yueyang, 414000, China, (corresponding author e-mail: 22017036@hnist.edu.cn).

Bin Li is an associate professor in College of Civil Engineering and Architecture, Hunan Institute of Science and Technology, Yueyang, 414000, China, (e-mail: 12007030@hnist.edu.cn).

Changqing Wu is a lecturer in College of Civil Engineering and Architecture, Hunan Institute of Science and Technology, Yueyang, 414000, China, (e-mail: 12021048@hnist.edu.cn).

Yongqing Zeng is a lecturer in College of Civil Engineering and Architecture, Hunan Institute of Science and Technology, Yueyang 414000, China, (e-mail: 1013433575@qq.com).

## I. INTRODUCTION

STEEL concrete composite box girders are advantageous due to their high stiffness, excellent torsional performance, and light self-weight, which are widely utilized in buildings and bridges [1], [2]. However, common like other types of box girders, the concrete slab in a steel-concrete composite box girder would undergo significant warping, which will result in an uneven stress distribution [3]. Such mechanical behavior is referred to as the shear-lag effect. It is evident that neglecting the shear lag effect can lead to significant underestimations of deformation and peak stresses, potentially causing the occurrence of cracks. Therefore, it is crucial to fully consider the impact of the shear lag effect on the steel-concrete composite box girders to ensure safety and reliability.

The shear lag effect in civil engineering structures was first recognized by Reissner [4], who utilized a predetermined warping function to describe the deformation of a box girder due to shear lag effect. Subsequently, there has been a proliferation of literature addressing the shear lag effect in steel-concrete composite box girders. V. Kristek [5] introduced a method for analyzing shear lag in steel and composite box girders of different cross-sectional types. Evans [6] extended the harmonic method to analyze girders with complex multicellular cross-sections and conducted a parametric study to illustrate the impact of specific parameters on the shear lag effect. Cheng [7], [8] applied the principle of virtual work to establish the differential equation for composite box girders, incorporating relative slip and shear lag effect. Li [9] investigated the distribution law of the effective width of a composite box girder bridge and developed a simplified analysis method for composite box girder bridges under bending and axial load. Hu [10] introduced a new double-box cross-section steel-concrete composite beam and conducted a theoretical analysis and experimental study to examine its stress behaviors, deflection characteristics, and the shear lag effect. Wang [11] derived an analytical expression for the shear lag effect in a simply supported composite box girder under a concentrated load at the midpoint of the span, assuming a parabolic warping displacement function. The difference in the shear lag and warping degrees of freedom functions between concrete slabs and steel girders was overlooked in the aforementioned studies, potentially leading to inaccuracies in the calculation results. Zhu [12] emphasized the independent shear lag and warping degrees of freedom functions for concrete slabs and steel beams and proposed a theoretical model that can directly account for the combined action of bending load and axial load. Henriques D [13] proposed a finite element

calculation model for steel concrete composite box beams based on the generalized beam theory, which can obtain accurate results with relatively few elements. Zhou [14] proposed a modified bar simulation method to analyze the shear lag effect of non-prismatic composite box girders with corrugated steel webs in the elastic stage. Zhu [15] developed a composite box girder finite element calculation model with 26 degrees of freedom, which can account for constrained torsion, distortion, shear lag, interface biaxial slip, and time-dependent effects. Zhao [16] proposed a finite beam element model for steel-concrete composite box girders, which accounts for slip, shear lag, and time-varying effects. Jiang [17] developed a theoretical method based on the energy variational principle to analyze the shear lag effect of the composite box girder bridges with corrugated steel webs. However, Jiang fails to account for some critical factors, such as the equilibrium condition of internal forces in the cross-section and the relationship between shear-lag warping displacement functions in different flanges. The research to date has tended to focus on theoretical and finite element analysis rather than experimental research. Additionally, few writers have been able to draw on any systematic parametric research.

The section that follows presents an experimental investigation of the shear lag effect in a steel-concrete composite box girder under bending moment and shear force, in which five load cases are designed. Subsequently, a detailed theoretical model for the composite girder is given, which accounts for the shear lag effect by using the warping function and incorporating the slip effect at the steel-concrete interface. Validation of the theoretical model is performed by comparing its results with the findings from the experimental tests. Furthermore, a parametric study is conducted to analyze the primary influencing factors on the shear lag effect using the proposed theoretical model. It is hoped that this research will contribute to offering a theoretical reference for the design of steel-concrete composite structures.

## II. THEORETICAL ANALYSIS

### A. Analysis Model

To facilitate the analysis, a Cartesian coordinate system is introduced, as depicted in Fig. 1. In the coordinate system, the  $x$ -axis is parallel to the composite girder. The longitudinal displacement at an arbitrary point in the concrete slab and in the U-shaped steel girder is denoted as  $u_c$  and  $u_s$ , respectively. The centroid of the concrete slab is represented as  $O_c$ , while that of the steel girder is denoted as  $O_s$ . The distance between  $O_c$  and  $O_s$  is denoted as  $h$ . Furthermore,  $O_{cs}$  represents the centroid of the equivalent section of the composite box girder. The distance from the neutral axis of the converted section of a composite girder to the centroidal axis of the concrete slab is represented as  $h_u$ , while  $h_L$  denotes the distance from the neutral axis of the converted section of a composite girder to the centroidal axis of the steel girder. Additionally,  $w$  represents the deflection of an arbitrary section of the composite girder, while  $\delta$  represents the relative slip at the interface of the composite girder. Lastly,  $\phi(x)$  denotes the relative rotation angle of the steel girder and the concrete slab.

The longitudinal displacement at an arbitrary point in the cross-section of a composite girder can be expressed as:

$$u(x, y, z) = u_1 + u_2 + u_3 \quad (1)$$

where:  $u_1$  represents the longitudinal displacement caused by the bending deformation of the composite girder itself;  $u_2$  indicates the longitudinal displacement caused by the interface slip of the composite girder;  $u_3$  represents the longitudinal displacement caused by the warping of the composite girder.

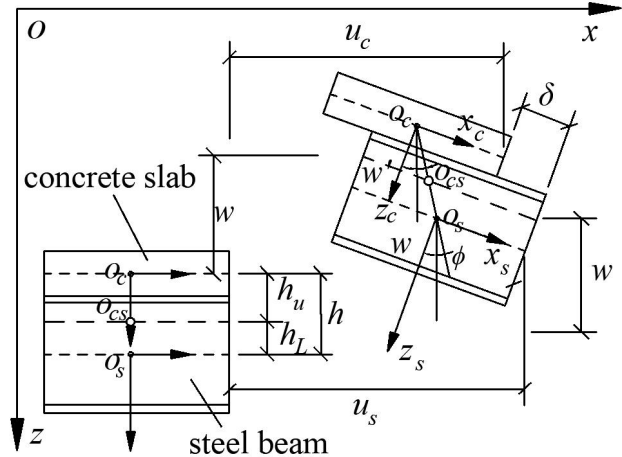


Fig. 1 Modeling of slip effect of composite box girder

### B. Warping displacement function

The warping displacement function could be described as the following:

$$u_3 = \psi(y)f(x) \quad (2)$$

where  $f(x)$  represents the strength function of the warping shape function along the longitudinal direction of the girder;  $\psi(y)$  represents the warping shape function.

The warping displacement function expressions of concrete inner top slab, concrete cantilever slabs, steel bottom slab, and steel webs slab could be described as the following:

$$\psi(y) = -\alpha_1(1 - y^2 / b_1^2) + D \text{ for top slab} \quad (3)$$

$$\psi(y) = -\alpha_2[1 - (b_1 + b_2 - y)^2 / b_2^2] + D \text{ for cantilever slabs} \quad (4)$$

$$\psi(y) = \alpha_3(1 - y^2 / b_3^2) + D \text{ for bottom slab} \quad (5)$$

$$\psi(y) = D \text{ for webs} \quad (6)$$

where  $D$  is the uniform axial displacement applied to satisfy the condition of axial force self-balancing. Additionally, the half-width of the concrete top slab is denoted as  $b_1$ , the width of the concrete cantilever slab as  $b_2$ , and the half-width of the steel bottom slab as  $b_3$ . Moreover, the shear lag warpage amplitudes of the concrete top slab, concrete cantilever slab, and steel bottom slab are denoted as  $\alpha_1$ ,  $\alpha_2$ , and  $\alpha_3$ , respectively. Supposing that  $\alpha_1 = 1$  for the concrete top slab, then

$$\alpha_2 = [8(1 + \mu)b_1^2b_2^2 + b_2^2L^2] / [8(1 + \mu)b_1^2b_2^2 + b_1^2L^2] \quad (7)$$

$$\alpha_3 = (b_3^2h_L) / (b_1^2h_u) \quad (8)$$

where  $\mu$  represents Poisson's ratio and  $L$  represents the calculated span of the composite girder.

According to the self-equilibrium condition of the warping stress, a uniform displacement was added along the axial direction of the girder, and the following condition must be satisfied

$$\int_A \psi(y) f'(x) dA = 0 \tag{9}$$

C. Displacement and Strain

The displacement of an arbitrary point in the cross-section of the concrete slab and steel girder under vertical load can be expressed as

$$\begin{Bmatrix} u_c \\ u_s \end{Bmatrix} = \begin{Bmatrix} -h_u & -z_c & 1 \\ h_L & -z_s & 1 \end{Bmatrix} \begin{Bmatrix} \phi \\ w' \\ \psi(y)f(x) \end{Bmatrix} \tag{10}$$

where  $z_c$  represents the z-coordinate value of an arbitrary point in the concrete slab relative to its centroidal axis;  $z_s$  represents the z-coordinate value of an arbitrary point in the steel girder relative to its centroidal axis.

The normal strain of an arbitrary point in the cross-section of the concrete slab and steel girder under vertical load can be expressed as

$$\begin{Bmatrix} \varepsilon_c = \frac{\partial u_c}{\partial x} \\ \varepsilon_s = \frac{\partial u_s}{\partial x} \end{Bmatrix} = \begin{Bmatrix} -h_u & -z_c & 1 \\ h_L & -z_s & 1 \end{Bmatrix} \begin{Bmatrix} \phi' \\ w'' \\ \psi(y)f'(x) \end{Bmatrix} \tag{11}$$

The shear strain of an arbitrary point in the cross-section of the concrete slab and steel girder under vertical load can be expressed as

$$\begin{Bmatrix} \gamma_c = \frac{\partial u_c}{\partial y} \\ \gamma_s = \frac{\partial u_s}{\partial y} \end{Bmatrix} = \begin{Bmatrix} 1 & 0 \\ 0 & 1 \end{Bmatrix} \begin{Bmatrix} \psi'(y)f(x) \\ \psi'(y)f(x) \end{Bmatrix} \tag{12}$$

D. Control differential equations and analytical solutions

According to the principle of virtual work, the total potential energy function under vertical load can be expressed as:

$$\begin{aligned} \Pi = & \int_L \int_{A_c} (E_c \varepsilon_c^2 / 2 + G_c \gamma_c^2 / 2) dA_c + \int_L K \delta^2 dx / 2 \\ & + \int_L \int_{A_s} (E_s \varepsilon_s^2 / 2 + G_s \gamma_s^2 / 2) dA_s + \int_L M(x) w'' dx \end{aligned} \tag{13}$$

where the elastic modulus of the steel girder and the concrete slab are denoted as  $E_s$  and  $E_c$ , respectively, while the shear modulus of the steel girder and the concrete slab are denoted as  $G_s$  and  $G_c$ , respectively. Furthermore, the composite girder's longitudinal shear stiffness per unit length at the interface is denoted as  $K$ . Additionally, the bending moment of any arbitrary section of the composite girder is represented as  $M(x)$ .

Substituting (6) and (9) into (10), we obtain the following equation:

$$\begin{aligned} \Pi = & \frac{1}{2} \{ B_1 \int_0^L (\phi')^2 dx + B_2 \int_0^L (w'')^2 dx + \\ & B_3 \int_0^L (f')^2 dx + B_4 \int_0^L \phi' f dx + B_5 \int_0^L f' w' dx + B_6 \int_0^L f^2 dx \\ & + C \int_0^L (\phi + w')^2 dx + 2 \int_0^L M(x) \cdot w'' dx \} \end{aligned} \tag{14}$$

where  $B_1 = \sum_{i=1}^2 E_c I_{cui} + E_s (I_{sL3} + I_{swL})$ ;

$$B_2 = \sum_{i=1}^2 E_c I_{ci} + E_s (I_{s3} + I_{sw})$$

$$B_3 = \sum_{i=1}^2 E_c A_{ci} (D^2 - 4\alpha_i D / 3 + 8\alpha_i^2 / 15) +$$

$$E_s A_{s3} (D^2 - 4\alpha_3 D / 3 + 8\alpha_3^2 / 15) + E_s A_{sw} D^2$$

$$B_4 = -4 \left( \sum_{i=1}^2 E_c S_{cui} \alpha_i + E_s S_{sL3} \alpha_3 \right) / 3 ; B_5 = -4 E_s S_{s3} \alpha_3 / 3 ;$$

$$B_6 = \sum_{i=1}^2 G_c A_{ci} 4\alpha_i^2 / (3b_i^2) + G_s A_{s3} 4\alpha_3^2 / (3b_3^2) ; C = K \cdot h^2 .$$

where  $I_{cui}$  represents the moment of inertia of the concrete top slab or cantilever slab about the neutral axis in the converted section,  $I_{sL3}$  represents the moment of inertia of the steel bottom slab about the neutral axis in the converted section, with the axis shifted to the centroid of the steel girder section. Similarly,  $I_{ci}$  represents the moment of inertia of the steel webs about the neutral axis in the converted section,  $I_{s3}$  represents the moment of inertia of the concrete inner slab or cantilever slab about its own neutral axis,  $I_{sw}$  represents the moment of inertia of the steel bottom slab about its own centroid axis,  $I_{swL}$  represents the moment of inertia of the steel web(including the upper flange) about its own neutral axis. Moreover, the cross-sectional area of the concrete inner slab or cantilever slab is represented as  $A_{ci}$ , while the cross-sectional area of the steel bottom slab is denoted as  $A_{s3}$ , and the cross-sectional area of the steel webs is represented as  $A_{sw}$ . Furthermore, the first moment of area of the concrete inner slab or cantilever slab about the neutral axis in the converted section is denoted by  $S_{cui}$ , while the first moment of area of the steel bottom slab about the neutral axis in the converted section, with the axis shifted to the centroid of the steel girder section, is indicated as  $S_{sL3}$ . Finally, the first moment of area of the bottom flange of the steel girder around its centroid is represented as  $S_{s3}$ .

We derived the differential equations and boundary conditions under vertical load through variational operation based on the principle of minimum potential energy, as follows:

$$B_2 w^{(3)} + B_5 f'' / 2 - C \phi - C w' + M'(x) = 0 \tag{15}$$

$$B_1 \phi'' + B_4 f'' / 2 - C \phi - C w' = 0 \tag{16}$$

$$B_3 f'' + B_4 \phi'' / 2 + B_5 w^{(3)} / 2 - B_6 f = 0 \tag{17}$$

$$(B_1 \phi' + B_4 f' / 2) \delta \phi \Big|_0^L = 0 \tag{18}$$

$$[B_2 w'' + B_5 f' / 2 + M(x)] \delta w \Big|_0^L = 0 \tag{19}$$

$$(B_3 f' + B_4 \phi' / 2 + B_5 w'' / 2) \delta f \Big|_0^L = 0 \tag{20}$$

By introducing the operator algorithm and combining (15), (16) and (17), we obtain the following differential equation:

$$J_1 f^{(4)} + J_2 f'' + J_3 f = J_4 Q(x) \tag{21}$$

where  $J_1 = 4B_1 B_2 B_3 - B_1 B_5^2 - B_2 B_4^2$ ;  $J_4 = 2C(B_4 - B_5)$ ;

$$J_2 = B_4^2 C - 2B_4 B_5 C + B_5^2 C - 4B_1 B_3 C - 4B_2 B_3 C - 4B_1 B_2 B_6 ;$$

$$J_3 = 4B_1 B_6 C + 4B_2 B_6 C .$$

Equation (21) can be written as

$$f^{(4)} + A_1 f'' + A_2 f = A_3 Q(x) \tag{22}$$

where  $A_1 = J_2 / J_1$ ;  $A_2 = J_3 / J_1$ ;  $A_3 = J_4 / J_1$ .

By solving the differential equation and substituting the corresponding boundary conditions under the applied load, we obtain the following equation:

$$f = C_1 \sinh(r_1 x) + C_2 \cosh(r_1 x) + C_3 \sinh(r_2 x) + C_4 \cosh(r_2 x) + A_3 Q(x) / A_2 \quad (23)$$

where  $r_1 = \sqrt{-2A_1 + 2\sqrt{A_1^2 - 4A_2}} / 2$ ;  $r_2 = \sqrt{-2A_1 - 2\sqrt{A_1^2 - 4A_2}} / 2$ .

By taking derivatives of (16) and (17), we obtain the following equation:

$$\begin{aligned} &-\frac{(B_1 B_5 + B_2 B_4)}{B_5} \frac{d^2 \phi(x)}{dx^2} + \frac{2B_2 B_6}{B_5} f(x) \\ &-\frac{1}{2} \frac{(B_4 B_5 - B_5^2 + 4B_2 B_3)}{B_5} \frac{d^2 f(x)}{dx^2} + Q(x) = 0 \end{aligned} \quad (24)$$

By substituting (23) into (24), we obtain the following solution:

$$\begin{aligned} \phi(x) = &Z_1 (C_1 \sinh(r_1 x) + C_2 \cosh(r_1 x)) \\ &+ Z_2 (C_3 \sinh(r_2 x) + C_4 \cosh(r_2 x)) \\ &+ \frac{(B_5 A_2 + 2B_2 B_6 A_3)}{A_2 (B_2 B_4 + B_1 B_5)} \iint Q(x) dx^2 + C_5 x + C_6 \end{aligned} \quad (25)$$

where  $Z_1 = -\frac{1}{2} \frac{(B_4 B_5 r_1^2 - B_5^2 r_1^2 + 4B_2 B_3 r_1^2 - 4B_2 B_6)}{(B_1 B_5 + B_2 B_4) r_1^2}$  ;

$$Z_2 = -\frac{1}{2} \frac{(B_4 B_5 r_2^2 - B_5^2 r_2^2 + 4B_2 B_3 r_2^2 - 4B_2 B_6)}{(B_1 B_5 + B_2 B_4) r_2^2}$$

According to the symmetry of the girder, the boundary conditions under the concentrated load  $P$  at the mid-span are as follows:

$$w(0) = 0, \phi'(0) = 0, w''(0) = 0, f'(0) = 0 \quad (26)$$

$$w'(L/2) = 0, f(L/2) = 0, \phi(L/2) = 0 \quad (27)$$

$$B_2 w'''(L/2) - Q(L/2) = 0 \quad (28)$$

By substituting (23) and (25) into (15), we obtain the following solution:

$$\begin{aligned} w(x) = &\frac{M_1}{r} (C_1 \cosh(r_1 x) + C_2 \sinh(r_1 x)) \\ &+ \frac{M_2}{r_2} (C_3 \cosh(r_2 x) + C_4 \sinh(r_2 x)) \\ &+ \frac{B_1 (2B_2 B_6 A_3 + B_5 A_2) P x}{2A_2 C (B_2 B_4 + B_1 B_5)} - \frac{1}{2} C_5 x^2 \\ &-\frac{1}{12} \frac{(2B_2 B_6 A_3 + B_5 A_2) P x^3}{A_2 (B_2 B_4 + B_1 B_5)} + C_6 x + C_7 \end{aligned} \quad (29)$$

where  $M_1 = \frac{B_1 Z_1 r_1^2}{C} + \frac{B_4 r_1^2}{2C} - Z_1$ ;  $M_2 = \frac{B_1 Z_2 r_2^2}{C} + \frac{B_4 r_2^2}{2C} - Z_2$ .

We derived the following equations from the boundary conditions:

$$C_1 = 0 \quad (30)$$

$$C_2 = \frac{\left[ (B_1 B_5^2 - 4B_1 B_2 B_3 + B_2 B_4^2) A_3 r_2^2 - 2B_1 B_5 A_2 \right] P}{2A_2 (B_1 B_5^2 - 4B_1 B_2 B_3 + B_2 B_4^2) (r_1^2 - r_2^2) \cosh\left(\frac{r_1 L}{2}\right)} \quad (31)$$

$$C_3 = 0 \quad (32)$$

$$C_4 = \frac{-\left[ (B_1 B_5^2 - 4B_1 B_2 B_3 + B_2 B_4^2) A_3 r_1^2 - 2B_1 B_5 A_2 \right] P}{2A_2 (B_1 B_5^2 - 4B_1 B_2 B_3 + B_2 B_4^2) (r_1^2 - r_2^2) \cosh\left(\frac{r_2 L}{2}\right)} \quad (33)$$

$$C_5 = 0 \quad (34)$$

$$C_6 = -Z_1 C_2 \cosh\left(\frac{r_1 L}{2}\right) - Z_2 C_4 \cosh\left(\frac{r_2 L}{2}\right) - \frac{\left( A_2 B_5 + 2B_2 B_6 A_3 \right) P L^2}{16A_2 (B_1 B_5 + B_2 B_4)} \quad (35)$$

$$C_7 = 0 \quad (36)$$

By substituting (23), (25), and (29) into (11), we obtain the normal strain at an arbitrary point in the cross section of composite girder under a vertical concentrated load at the mid-span.

### III. EXPERIMENTAL STUDY

#### A. Description of specimen

A static loading test is conducted to investigate the shear lag effect in a simply supported steel-concrete composite box-girder with straight steel webs.

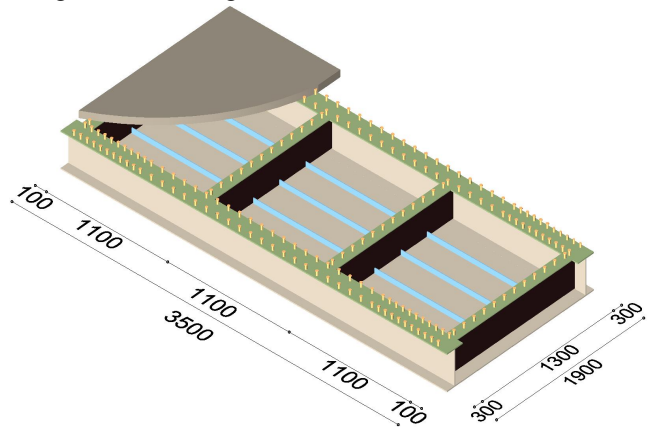


Fig. 2 Overall view of steel-concrete composite girder(unit:mm)

As shown in Fig. 2, the specimen consists of a longitudinal steel U-shaped girder, four transverse steel I-shaped beams, and a reinforced concrete (RC) concrete slab. Dimension of the specimen is illustrated in Fig. 3. The depth of the steel U-shaped girder is 300 mm. The distance between two straight steel webs is 1300 mm ( $2b_1$ ) and the spacing of transverse steel I-shaped beams is 1100 mm, as illustrated in Fig. 3(a). The total span of the specimen is 3500 mm (3300 mm for calculated span  $L$ ), with a height of 360 mm, as shown in Fig. 3(b). Additionally, the width and thickness of the RC concrete slab ( $h_c$ ) are 1900 mm and 60 mm, respectively, as depicted in Fig. 3(c).

Furthermore, the RC concrete slab is connected to the steel girder using shear studs. The diameter and height of the studs are 16 mm and 50 mm, respectively. Double-line studs are welded onto the top flange of longitudinal steel U-shaped girder, whereas single-line studs are welded onto the top flange of the transverse steel I-shaped beams, as depicted in Fig. 3(d).

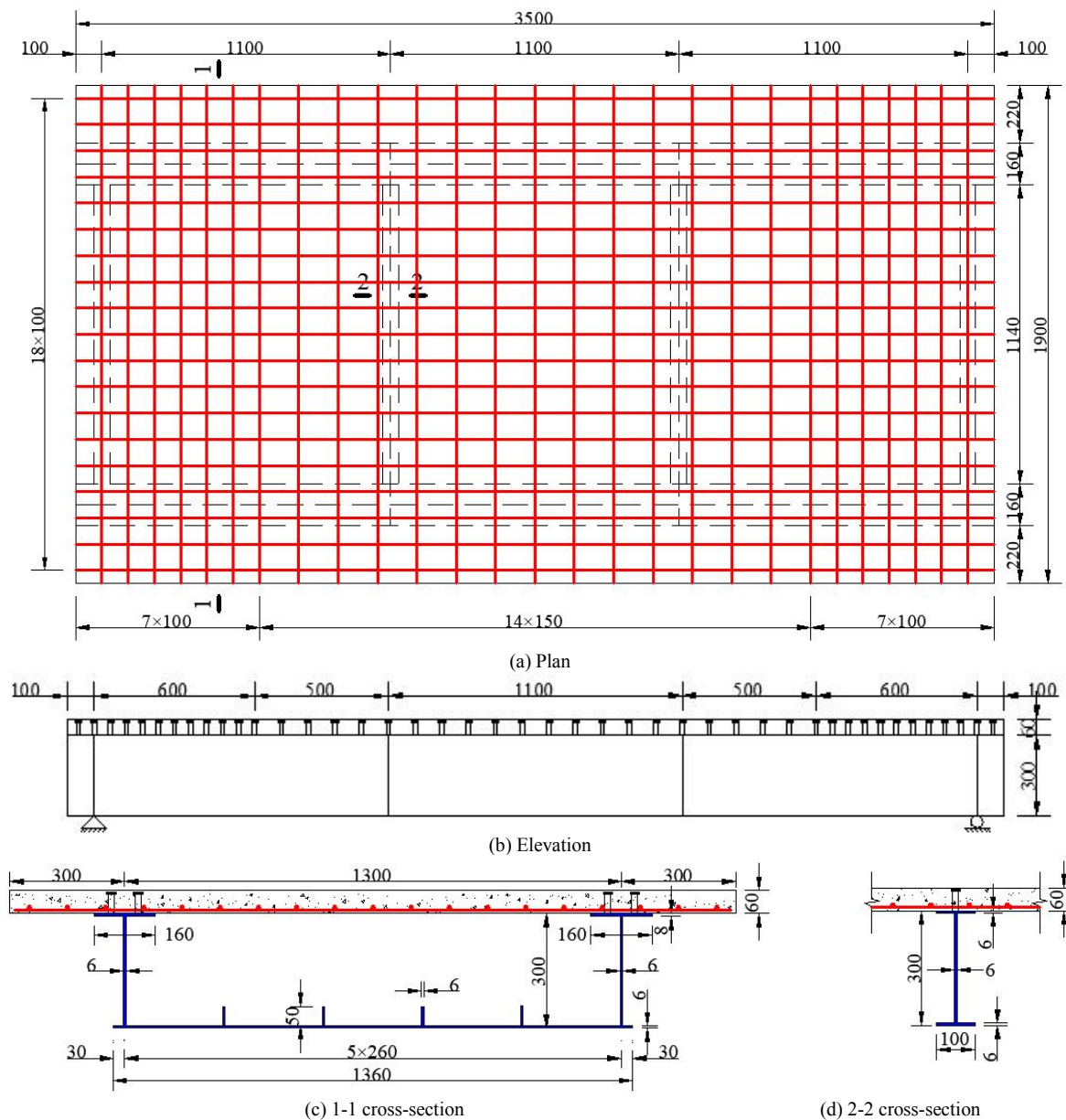


Fig. 3 Dimension of the specimen(unit:mm)

The spacing of the studs welded onto steel U-shaped girder is initially 110 mm, but is reduced to 60 mm within the range of 600 mm from the girder ends, as indicated in Fig. 3(b). Meanwhile, the studs welded onto the transverse beams are spaced at 60 mm.

**B. Material properties**

In the girder specimen, C50 concrete is used for the concrete slab, Q355b steel is used for the steel U-shaped girder and transverse steel I-shaped beams, and Q245 steel bar with a diameter of 12mm is used for the reinforcement in the concrete slab. The concrete strength is determined by concrete cubic tests in accordance with Chinese Standard GB/T 50152-2012 [18]. The compressive strengths of six concrete cubic specimens are as follows: 61.05 MPa, 59.18 MPa, 58.91 MPa, 61.14 MPa, 57.59 MPa, and 58.37 MPa, respectively, and the average cubic compressive strength is 59.37 MPa.

**C. Experimental set-up and procedures**

The fabrication of the specimen is shown in Fig. 4. The steel girder is manufactured in a steel structure processing factory. The steel components are transported to the Structural Laboratory of Hunan Institute of Science and Technology for formwork support and on-site pouring of concrete. The specimen was simply supported by steel pins and rollers 100mm away from the ends of the girder. The static test is carried out utilizing an electric-hydraulic serve testing machine and the vertical concentrated-load on the mid-span of the specimen is applied by a hydraulic jack, as shown in Fig. 5. The test covered five load cases, as detailed in Table I. In this test, the strain gauges are arranged at the designated position, as indicated in Fig. 6. To measure the transverse distribution of the normal strain, strain gauges are placed on the upper surface of the concrete slab with a transverse spacing of 130 mm along the slab width. Additionally, the  $L/2$  section and  $L/4$  section of the specimen were identified as the control cross-sections.



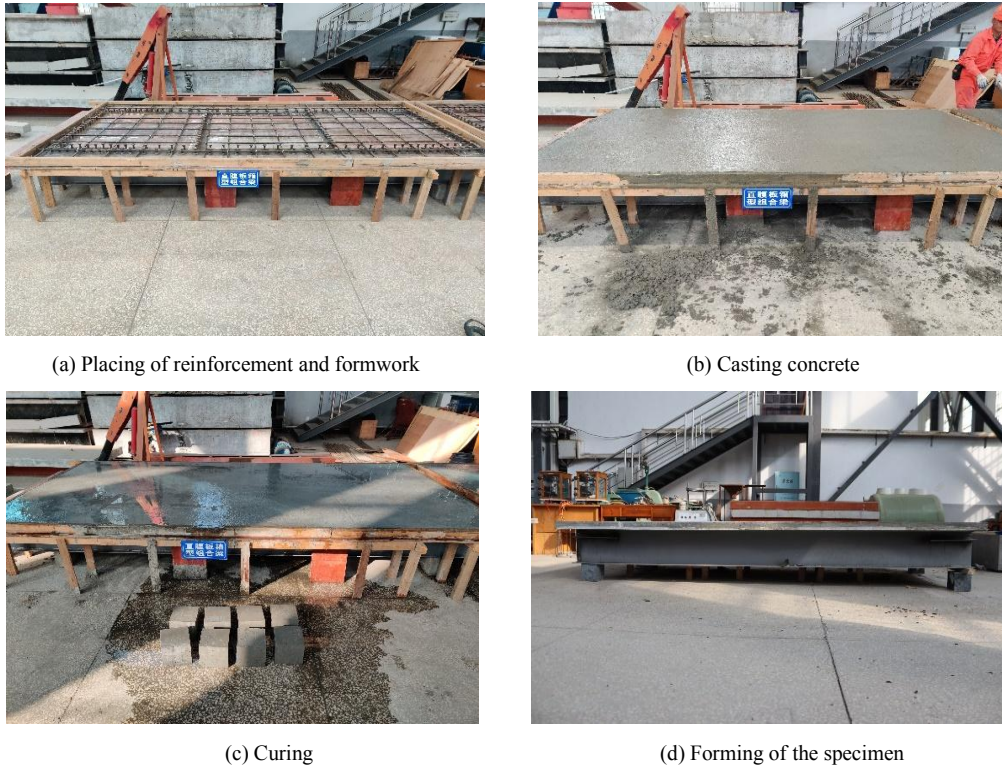


Fig. 4 Fabrication of the specimen

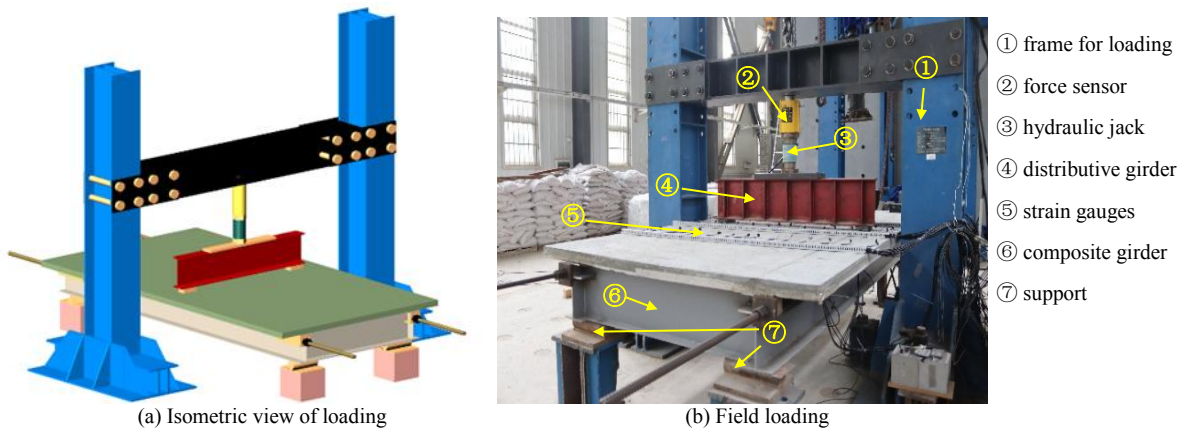


Fig. 5 Loading arrangement for the specimen

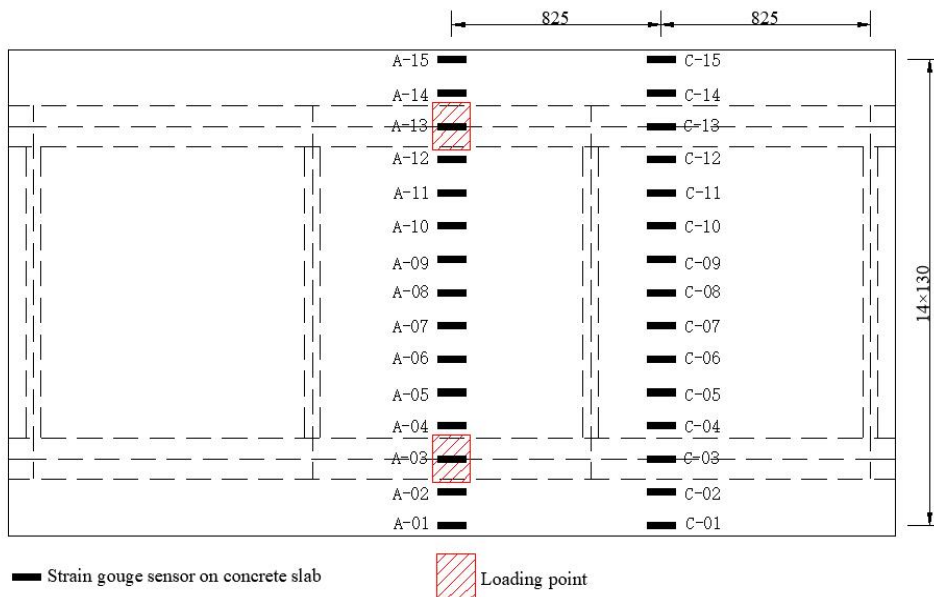
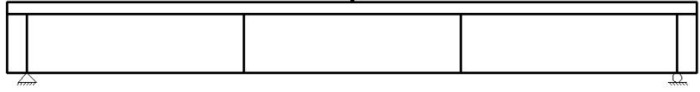


Fig. 6 Layout of sensors(unit:mm)

TABLE I  
SPECIMEN LOAD CASES

Case No.	Loading configuration	Vertical load (kN)
1		50
2		75
3		100
4		125
5		150

D. Experimental results

The strains are measured at the  $L/4$  and  $L/2$  sections, as shown in Fig. 7. From the data in Figure 7, we can see a positive correlation between the strain values and the load values. The characteristic of strain distribution at the  $L/2$  section is similar to that at the  $L/4$  section. Both the  $L/4$  section and  $L/2$  section reveal non-uniform strain distribution, and the strains reach their maximum at web-flange junction. However, notable differences have been found in the rate of decline of strains between the  $L/4$  section and the  $L/2$  section. The shear lag coefficient value of the concrete slab at the  $L/2$  section ranges from 1.382 to 1.455, whereas at the  $L/4$  section, it ranges from 1.095 to 1.136. It indicates that the shear lag phenomenon is more pronounced at the  $L/2$  section than at the  $L/4$  section, suggesting that the section closer to the loading point exhibits a more pronounced shear lag phenomenon.

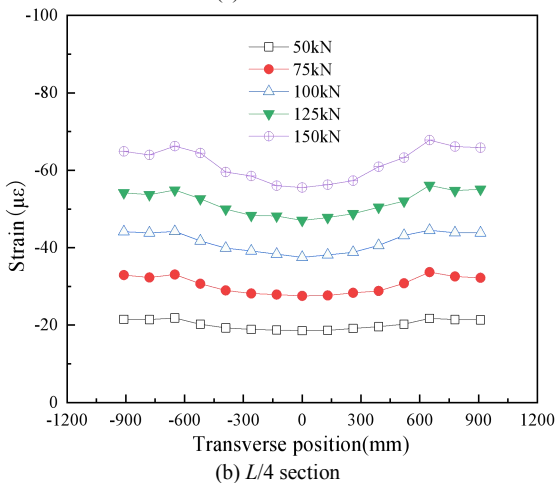
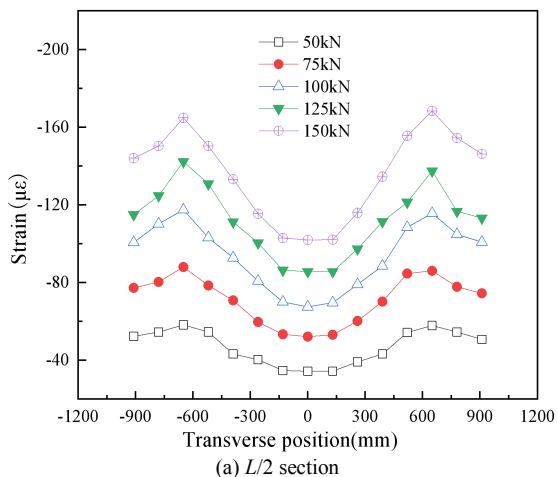
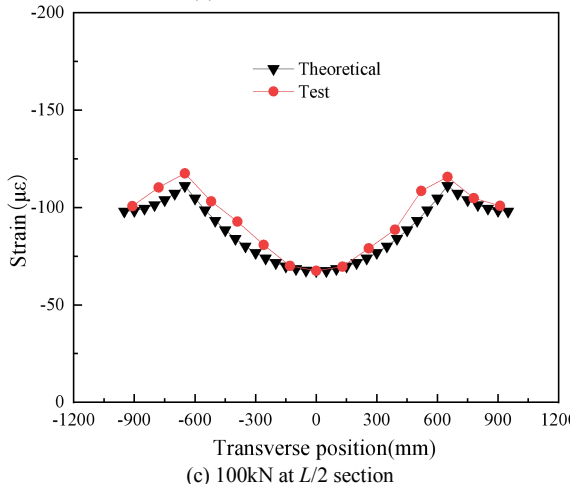
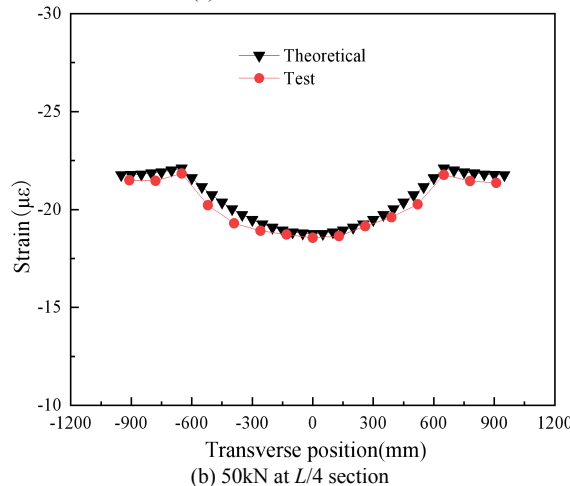
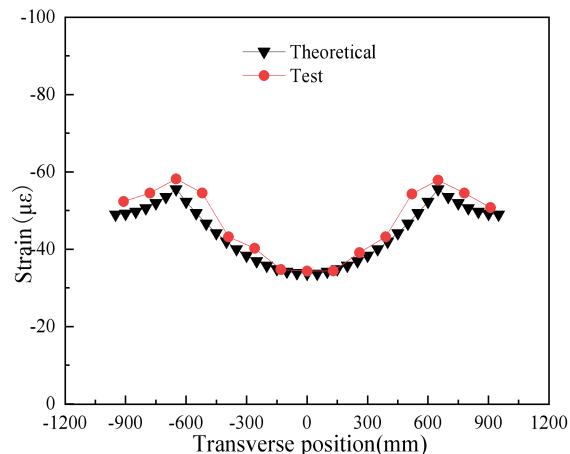


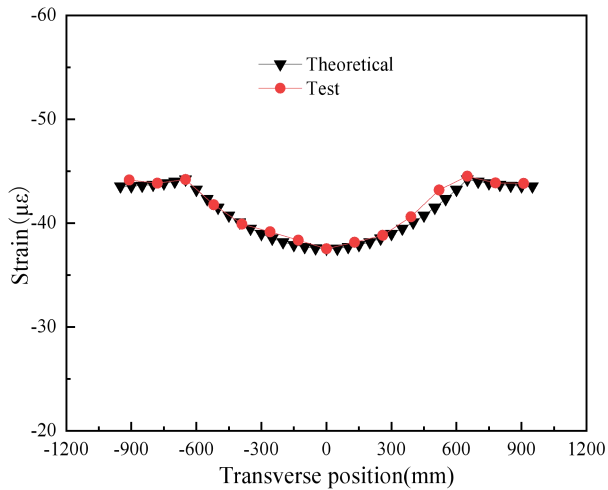
Fig. 7 Strains on top surface of concrete slab

E. Analytical validation

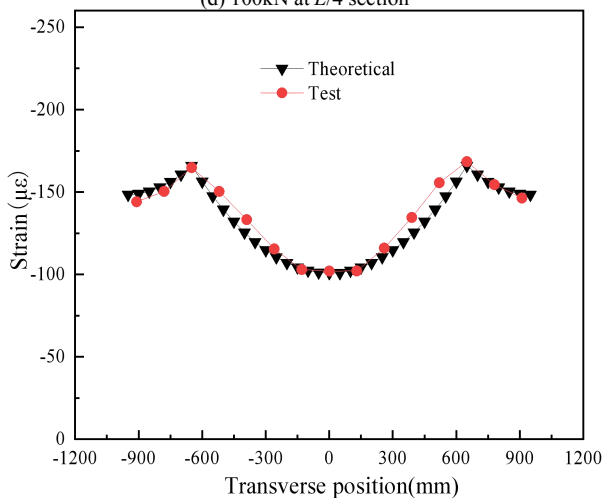
A comparative analysis of longitudinal strains is conducted to validate the theoretical model's applicability within the

linear elastic range, as depicted in Fig. 8. The normal strain distribution between the theoretical solution and experimental results demonstrates consistency. The maximum difference between the theoretical and experimental results falls within the range of 0.4-15.5%, and the average difference is 5.6%. The applicability of the theoretical model is calibrated.

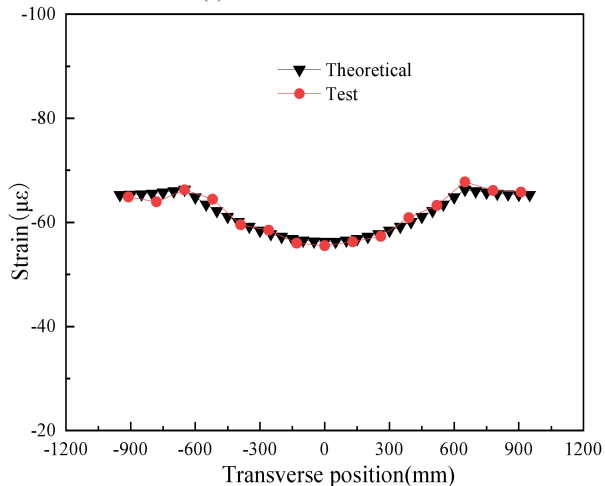




(d) 100kN at L/4 section



(e) 150kN at L/2 section



(f) 150kN at L/4 section

Fig. 8 Results comparison

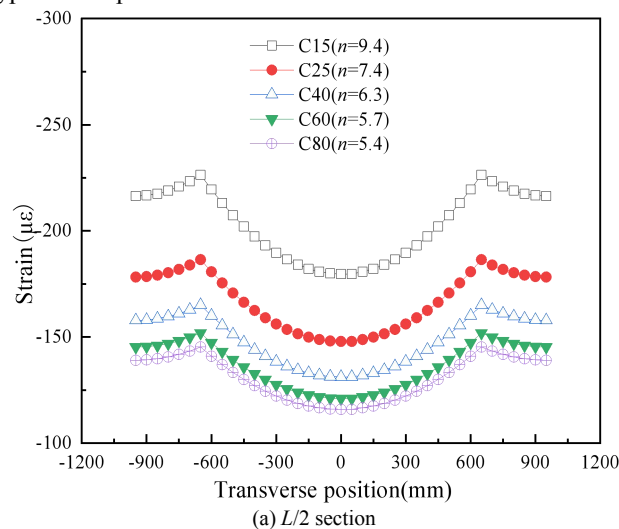
#### IV. PARAMETRIC ANALYSIS

Following the theoretical analysis and experimental investigation discussed above, the related parameter impact analysis is also carried out based on the above specimen model. Six parameters are considered: (a) the modulus ratio( $n$ ) ranging from 5.4 to 9.4; (b) the concrete slab thickness ranging from 60mm to 120mm; (c) the calculated span ranging from 1800mm to 4200mm; (d) the ratio of the cantilever slab width to the half-width of top slab ( $b_2/b_1$ ) ranging from 0.5 to 1.5; (e) the thickness of steel flange plate ranging from 8mm to 40mm; (f) the thickness of steel web

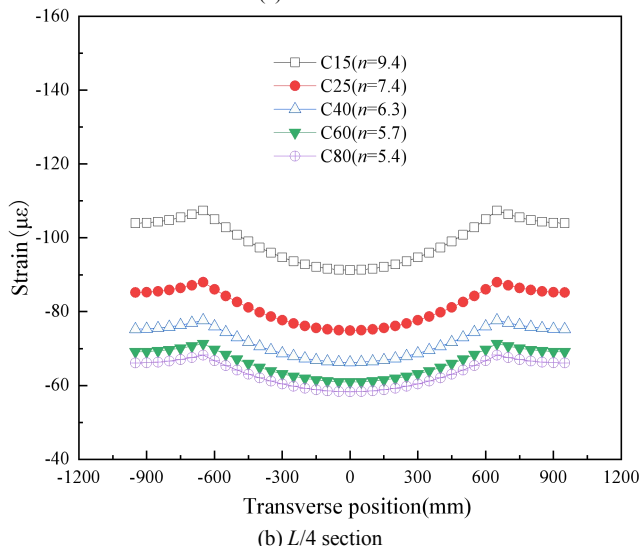
plate ranging from 6mm to 30mm. In order to prevent interference between parameters, each parameter is examined while the others are kept constant. The theoretical model is used to conduct the comprehensive parametric analysis.

##### A. Impact Analysis for Modulus Ratio

The concrete strength is designed as C15, C25, C40, C60, and C80 to conduct parametric sensitivity analysis on the shear lag effect. The strain distribution on the top surface of concrete under  $n=\{9.4, 7.4, 6.3, 5.7, 5.4\}$  is obtained. As depicted in Fig. 9, an ascending trend in strain can be observed with the increasing modulus ratio at both the  $L/2$  and  $L/4$  sections. Concurrently, the shear lag coefficient of the concrete slab exhibits a diminishing trend, decreasing from 1.385 to 1.379 at the  $L/2$  section and from 1.121 to 1.095 at the  $L/4$  section. It further contends that the modulus ratio has an insignificant impact on the shear lag effect in this type of composite structure.



(a) L/2 section



(b) L/4 section

Fig. 9 Longitudinal strain distribution on top surface of concrete slab across slab width for different  $n$

##### B. Impact Analysis for Concrete Slab Thickness

The thickness of the concrete slab is a critical parameter influencing the shear lag of the composite girder. The slab thicknesses are defined as 60 mm, 75 mm, 90 mm, 105 mm, and 120 mm, respectively, as shown in Fig. 10. Increasing the slab thickness can mitigate the shear lag effect, as it enhances the uniformity of the interface stiffness of composite girders



and reduces the relative slip between steel beams and concrete slabs. With the increase in thickness from 60 mm to 120 mm, the shear lag coefficient at the  $L/2$  section decreases from 1.384 to 1.300, and at the  $L/4$  section, it decreases from 1.099 to 1.028. However, it is essential to note that augmenting the slab thickness will lead to an increase in the girder's self-weight and cost, which may have unfavorable implications. Therefore, a comprehensive consideration of multiple factors is essential in the design process.

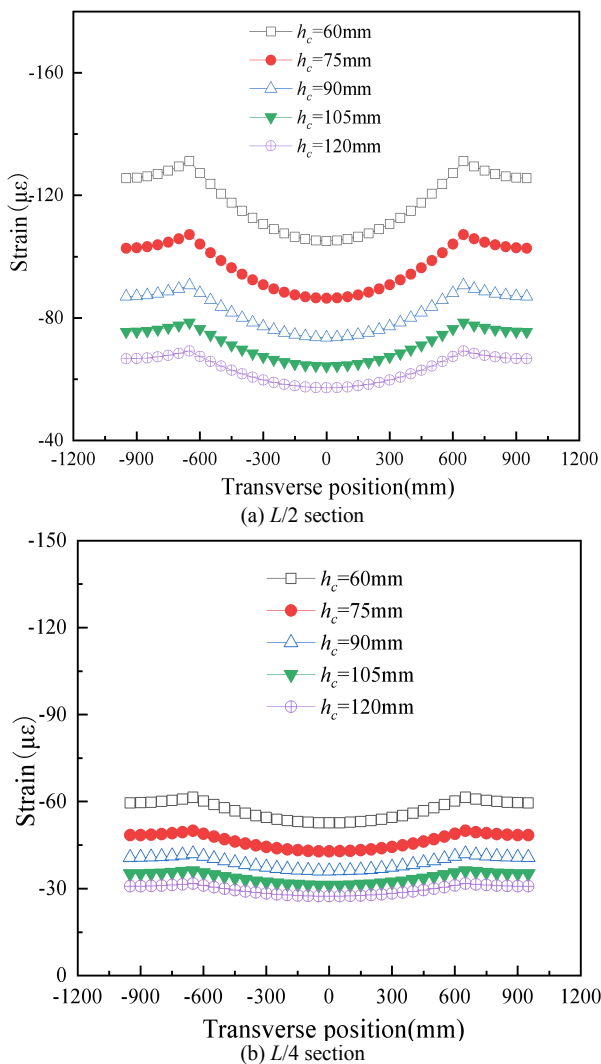


Fig. 10 Longitudinal strain distribution on top surface of concrete slab across slab width for different concrete slab thickness

C. Impact Analysis for Calculated Span

The calculated spans for exploring parametric sensitivity are defined as 1800 mm, 2400 mm, 3000 mm, 3600 mm, and 4200 mm, respectively, as shown in Fig. 11. In Fig. 11(a), the strain distribution reveals a linear increase at the  $L/2$  section as the calculated span increases. In Fig. 11(b), at the  $L/4$  section, the strain distribution on the top surface of the concrete becomes progressively more uniform with the increasing span, which is further correlated with the increasing distance from the loading point. Additionally, the shear lag coefficient of the concrete slab demonstrates a decreasing trend from 1.411 to 1.046 as the span increases from 1800 mm to 4200 mm. The results indicate that the calculated span has a significant influence on shear lag effect.

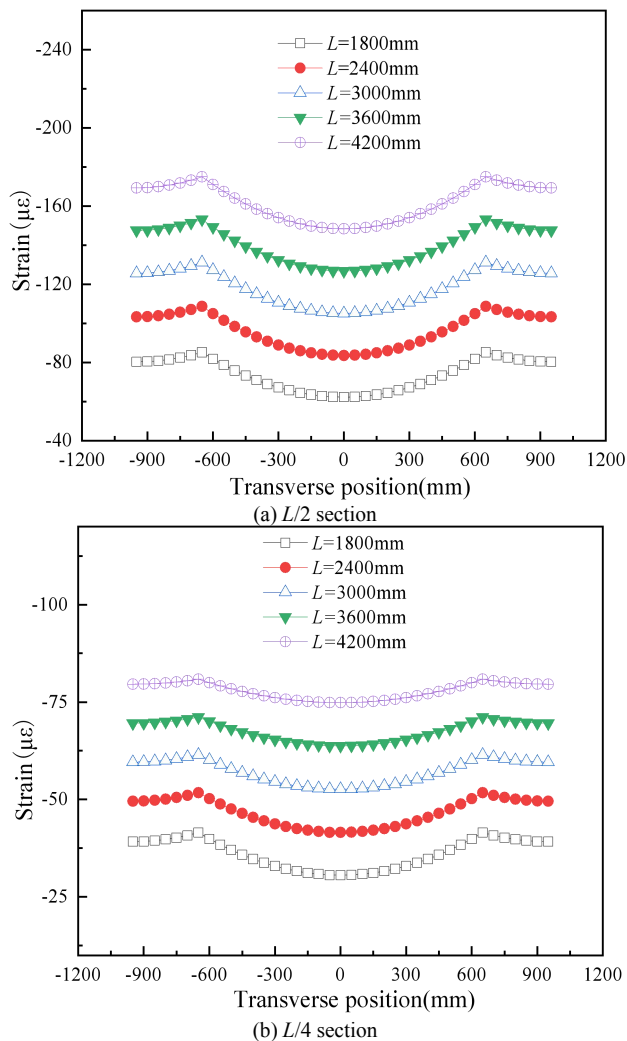
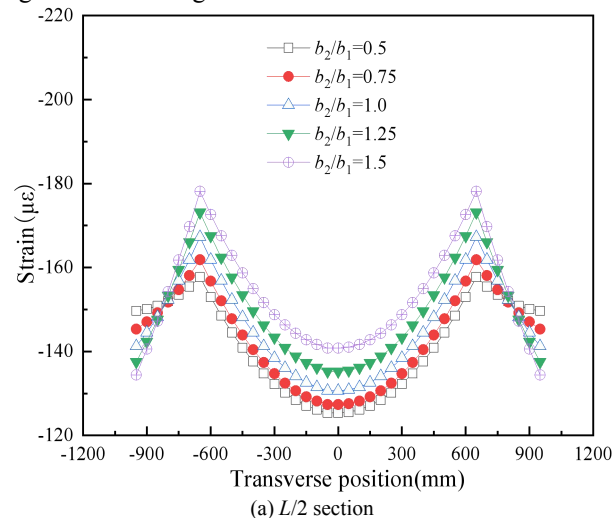


Fig. 11 Longitudinal strain distribution on top surface of concrete slab across slab width for different span

D. Impact Analysis for  $b_2/b_1$  Ratio

Fig. 12 depicts the longitudinal strain distribution variations on the top surface of the concrete slab under different  $b_2/b_1$  ratios. It is evident that an increase in the  $b_2/b_1$  ratio has an insignificant impact on the shear lag effect when it is less than 1. However, as the  $b_2/b_1$  ratio exceeds 1, the shear lag effect becomes more pronounced, signifying a correlation between the increasing  $b_2/b_1$  ratio and the heightened shear lag effect.



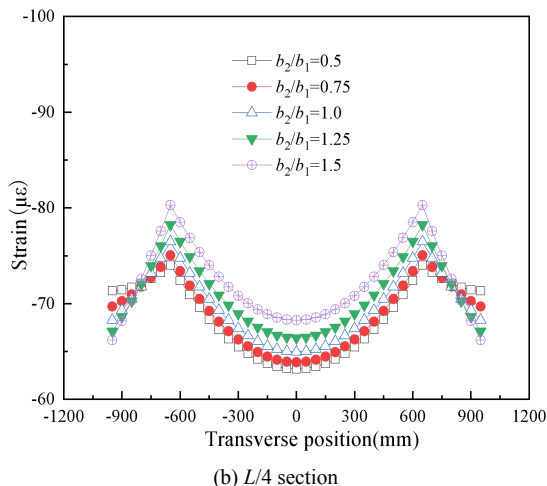


Fig. 12 Longitudinal strain distribution on top surface of concrete slab across slab width for different  $b_2/b_1$  ratio

E. Impact Analysis for Thickness of Steel Flange Plate

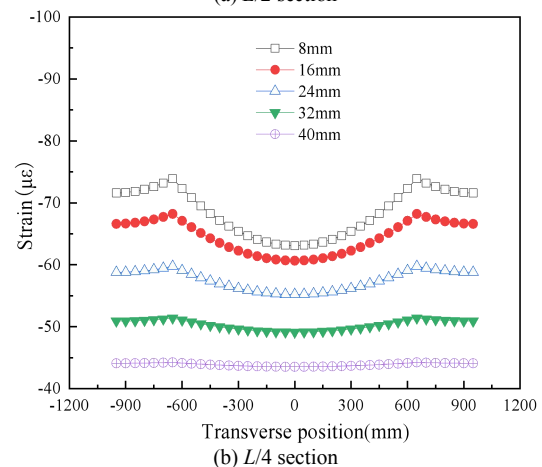
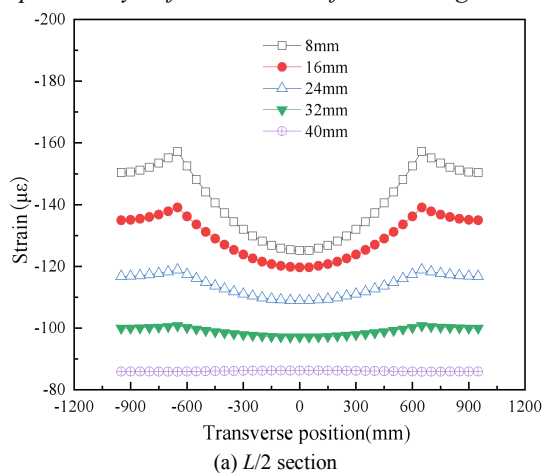


Fig. 13 Longitudinal strain distribution on top surface of concrete slab across slab width for different thickness of steel flange plate

Five different steel flange plate thicknesses are set as follows: 8mm, 16mm, 24mm, 32mm, and 40mm. The influence of the thickness of steel flange plate on shear lag behavior is displayed in Fig. 13. A significant shear lag effect can be observed when the flange plate thickness is within three times the initial thickness (8mm). With the increase in thickness from 8mm to 40mm, the shear lag coefficient of the concrete slab at the  $L/2$  section decreases from 1.384 to 1.002, and at the  $L/4$  section decreasing from 1.099 to 1.001, resulting in a more uniform strain across the concrete slab. It indicates the significant impact of the steel flange plate thickness on the shear lag effect. Nevertheless, the

augmentation of the steel flange plate thickness also leads to increased self-weight, potentially causing an uneven strain distribution longitudinally and ensuing lateral buckling of the steel plate. Consequently, a comprehensive consideration of all pertinent factors is essential for devising the optimal design scheme.

F. Impact Analysis for Thickness of Steel Web Plate

Five different steel web plate thicknesses are set as follows: 6mm, 12mm, 18mm, 24mm, and 30mm. The influence of the thickness of the steel web plate on shear lag behavior is displayed in Fig. 14. A marginal decrease is revealed in the shear lag coefficient of the concrete slab, with values reducing from 1.384 to 1.362 at the  $L/2$  section and from 1.099 to 1.075 at the  $L/4$  section. It further indicates that the aforementioned thickness of the steel flange plate has a more significant effect on the shear lag effect than the thicknesses of the steel web plate.

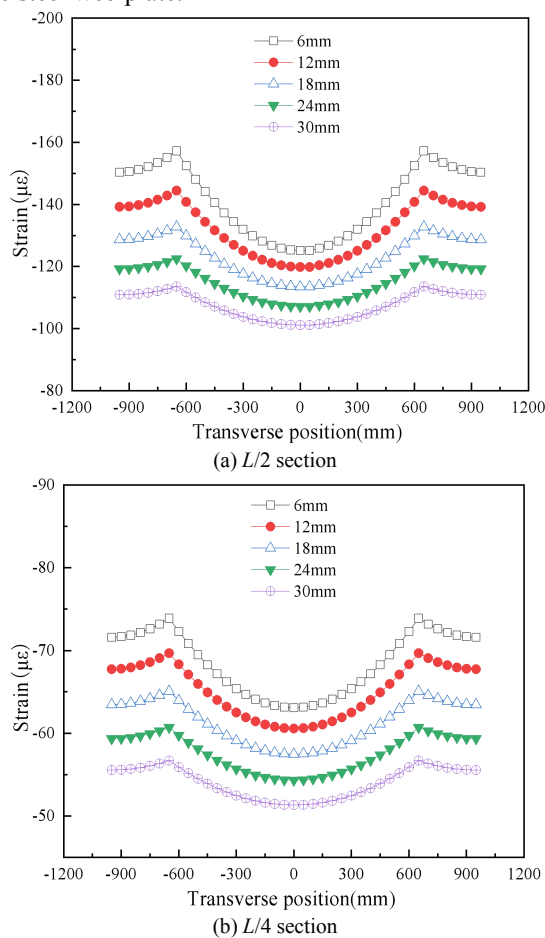


Fig. 14 Longitudinal strain distribution on top surface of concrete slab across slab width for different thickness of steel web plate

V. CONCLUSION

This study aims to investigate the shear lag effect of the concrete slab in composite box girders with straight steel webs through experimental and analytical methods. A composite girder specimen is designed and tested. A theoretical model for composite girders is developed, which used the warpage function and considered the slip effect at the steel-concrete interface. A parametric sensitivity analysis on the shear lag behavior is conducted to investigate the impact of six key parameters: modulus ratio, concrete slab thickness, calculated span, the ratio of cantilever slab width to half-width of the top slab, thickness of the steel flange

plate, and thickness of the steel web plate. Based on the present study, the following conclusions could be drawn:

(1) In the experimental study, the strain distributions reveal an apparent shear lag effect in the concrete slabs of the specimen. A positive correlation between the strain values and the load values is found. The characteristic of strain distribution at the  $L/2$  section is similar to that at the  $L/4$  section. Particularly, the shear lag coefficient value of the concrete slab at the  $L/2$  section ranges from 1.382 to 1.455, whereas at the  $L/4$  section, it ranges from 1.095 to 1.136. These findings indicate that the distance from the loading point notably influences the strain distribution characteristic.

(2) The theoretical model is used to calculate the normal strains on the top surface of the concrete slab, which are found to closely match the corresponding experimental results. Particularly, the normal strains calculated by the theoretical model closely match the experimental results, with an average difference of 5.6%, which empirically supports the validity of the proposed theoretical model.

(3) The parametric analysis indicates that the influence of the modulus ratio on the shear lag coefficient can be ignored. The thickness of the concrete slab is a critical parameter influencing the shear lag. One of the more significant findings to emerge from the parametric analysis is that the shear lag effect becomes more pronounced when the  $b_2/b_1$  ratio exceeds 1, therefore, a small  $b_2/b_1$  ratio should be adopted to avoid a severe shear-lag effect. Furthermore, the study indicates that the shear-lag effect in a composite box girder increases proportionately to the calculated span. Additionally, the thickness of the steel flange plate exerts a more pronounced influence on the shear lag effect than the thicknesses of the steel web plate.

In summary, this study makes critical theoretical contributions to understanding and analyzing the shear lag phenomenon in steel-concrete composite box girders with straight steel webs. The integrated experimental and analytical validations provide robust tools for engineering design. The research enhances knowledge of shear lag behavior and demonstrates the need to properly account for its effects in the analysis and design of composite structures. However, this study solely investigates the shear lag effect of the composite girder within a linear elastic range, and more research is required to explore its nonlinear features.

#### REFERENCES

- [1] Chen, H., Zeng, J., Zhao, H., and Liu, X. "Bond-slip effect in novel steel box-concrete composite structures part I : Short-term loading," Structures, vol.51, pp1450-1460, 2023
- [2] Bimo B. Adhitya, Anthony Costa, Kencana Verawati, and Wadirin, "Study on the Failure Performance of Reinforced Concrete and Composite Concrete Structures due to Non-Linear Time History Earthquake Loads," Engineering Letters, vol.31, no.2, pp544-553, 2023
- [3] Tesfaldet Gebre, Vera Galishnikova, and Evgenia Tupikova, "Warping Behavior of Open and Closed Thin-Walled Sections with Restrained Torsion," Engineering Letters, vol.30, no.1, pp354-361, 2022
- [4] Reissner, and Eric. "Analysis of shear lag in box beams by the principle of the minimum potential energy," Quarterly of Applied Mathematics, vol.4, no.3, pp268-278, 1946
- [5] V. Kristek, H.R. Evans, and M.K.M. Ahmad, "A shear lag analysis for composite box girders," Journal of Constructional Steel Research, vol.16, no.1, pp1-21, 1990
- [6] R H. Evans, KH M.Ahmad, and V.Kristek, "Shear lag in composite box girders of complex cross-sections," Journal of Constructional Steel Research, vol.24, no.3, pp183-204, 1993
- [7] HG Cheng, and SZ Qiang, "Shear Lag Analysis of Steel-concrete Composite Box Girder in Consideration of Relative Slippage," China Railway Science, vol.24, no.6, pp49-52, 2003 (in Chinese)
- [8] HG Cheng, and SZ Qiang, "Series solution of shear lag of steel-concrete composite box girder," China Civil Engineering Journal, vol.37, no.9, pp37-40, 2004 (in Chinese)
- [9] Li Faxiong and Nie Jianguo, "Elastic analytical solutions of shear lag effect of steel-concrete composite beam," Engineering Mechanics, vol.28, no.09, pp1-8, 2011 (in Chinese)
- [10] S.W. Hu, J. Yu, Y.Q. Huang, and S.Y. Xiao, "Theoretical and Experimental Investigations on Shear Lag Effect of Double-Box Composite Beam with Wide Flange under Symmetrical Loading," Journal of Mechanics, vol.31, no.6, pp653-663, 2015
- [11] Wang Lianguang, and Wan Jiang, "Analysis of shear lag effect of steel and concrete composite box girders," Journal of Northeastern University (Natural Science), vol.36, no.08, pp1204-1207+1216, 2015 (in Chinese)
- [12] Zhu Li, Nie Jianguo and Ji Wenyu, "Slip and shear-lag effects of steel-concrete composite box beam," Engineering Mechanics, vol.33, no.09, pp49-58+68, 2016 (in Chinese)
- [13] David Henriques, Rodrigo Gonçalves, Carlos Sousa, and Dinar Camotim, "GBT-based time-dependent analysis of steel-concrete composite beams including shear lag and concrete cracking effects," Thin-Walled Structures, vol.150, pp106706, 2020
- [14] Cong Zhou, Lifeng Li, and Jianqun Wang, "Modified bar simulation method for shear lag analysis of non-prismatic composite box girders with corrugated steel webs," Thin-Walled Structures, vol.155, pp106957, 2020
- [15] Li Zhu, Ray Kai-Leung Sub, and Ming-Jie Li, "Finite beam element with 26 DOFs for curved composite box girders considering constrained torsion, distortion, shear lag and biaxial slip," Engineering Structures, vol.232, pp111797, 2021
- [16] GuanYuan Zhao,Wei Liu,Rui Su, and Jia Cheng Zhao, "A Beam Finite Element Model Considering the Slip, Shear Lag, and Time-Dependent Effects of Steel-Concrete Composite Box Beams," Buildings, vol.13, no.1, pp13010215, 2023
- [17] Ruijuan Jiang, Qiming Wu, Yufeng Xiao, Manlin Peng, Francis Tat Kwong Au, Tianhua Xu, and Xiachun Chen, "The shear lag effect of composite box girder bridges with corrugated steel webs," Structures, vol.48, pp1746-1760, 2023
- [18] GB/T 50152-2012, Standard for test method of concrete structures, China Architecture & Building Press, 2012, (in Chinese).



**Dr. Hua Luo** was born in September 1985 and received her Ph.D. Degree from Beijing Jiaotong University, Beijing, China, in 2015. She is an associate professor in College of Civil Engineering and Architecture, Hunan Institute of Science and Technology, Yueyang, China. Her research interests cover bridge engineering and composite structure. She has published more than 20 technical papers.



**Jianqiang Feng** was born in December 1998 and received his B.E. Degree from Hunan Institute of Science and Technology, Yueyang, China, in 2021. His research interest is mainly on the shear lag effect of steel-concrete composite girders. Jianqiang Feng is a postgraduate student in Hunan Institute of Science and Technology. He has authored or co-authored 2 journal papers.



**Mr. Qincong She** was born in July 1987 and received his M.S. Degree from Changsha University of Science and Technology, Changsha, China, in 2014. His research interests are mainly on bridge construction monitoring and steel-concrete composite structure. Qincong She has worked as a lecturer in Hunan Institute of Science and Technology. He has authored or co-authored 6 journal papers to date.



**Dr. Bin Li** was born in December 1981 and received his Ph.D. Degree from Changsha University of Science and Technology, Changsha, China, in 2017. He is an associate professor in College of Civil Engineering and Architecture, Hunan Institute of Science and Technology, Yueyang, China. His research interests cover bridge engineering and engineering mechanics. He has published more than 30 technical papers.